CSMA 2019
14ème Colloque National en Calcul des Structures
13-17 Mai 2019, Presqu'île de Giens (Var)

A Multiscale Modeling on Shape Memory Alloy Based Cellular Materials

R. Xu[1,2], C. Bouby[1], H. Zahrouni[2], T. Ben Zineb[2], H. Hu[1], M. Potier-Ferry[2]

[1] *School of Civil Engineering, Wuhan University, {ruixu,huheng}@whu.edu.cn*
[2] *LEM3, Université de Lorraine, {celine.bouby,hamid.zahrouni,tarak.ben-zineb,michel.potier-ferry}@univ-lorraine.fr*

Abstract — In this paper, the superelasticity effects of architected *shape memory alloys* (SMAs) are studied by the *multilevel finite element method* (FE^2), which couples the responses of both the cellular level and structural level by considering their real-time information interactions. Firstly, a parametric analysis for the void fraction, the total stiffness, the hysteresis effect and the mass of the SMAs is conducted at the cellular level. Then, through a multiscale three point bending test, it is observed that the structure inherits both the hysteresis effect and the superelasticity from the architected cellular SMAs.
Keywords — shape memory alloys, architected cellular material, numerical homogenization.

1 Introduction

Architected cellular materials are widely used for their high strength-to-weight ratio and high energy absorption performance. Thanks to the highly developed additive manufacturing techniques, such as 3D printing (Ngo et al. [1]; Mostafaei et al. [2]), the manufacturing of architected cellular materials is no longer impossible. Users can design a cellular material with a certain behavior by tuning its cellular parameters, such as the geometry, components, local material properties, etc.

Architected cellular materials' functionality could be extended by combining the features of various materials, such as *shape memory alloys* (SMAs). It is well known that shape memory alloys, such as NiTi, can endure large deformation and recover their initial shape after unloading (see for example the reviews of Patoor et al. [3], Lagoudas et al. [4] and Cisse et al. [5]). This superelasticity effect brings high performance to SMA in energy absorption. When the given load reaches a critical level in a superelastic test, SMA will apparently soften due to its inner phase transformation. This behavior enables SMA to absorb the external energy as much as possible and prevents material from crushing or buckling. Such a kind of response is very similar to the ideal response of the cellular material designed by Schaedler et al. [6]. Meanwhile, the hysteresis effects of SMA can dissipate a large amount of energy. All mentioned features of SMAs meet the requirements of an architected structure for energy absorption applications very well. In addition, taking advantage of the lightweight and shape memory effect, architected SMAs may be designed for advanced applications in aerospace, civil engineering, etc.

Considering the scale separation between the microscopic cellular scale and macroscopic structural scale, however, it is difficult to predict the structural response by a unit cell, because the stress-strain states of the macroscopic structure are usually not uniform and the deformations at the microscopic level could be totally different. Thus, it is therefore necessary to investigate the behavior of architected SMAs with a *multilevel finite element* (FE^2) model [7, 8]. In this work, FE^2 is adopted, which shows good performance on multiscale modeling of SMA-based materials [9, 10]. Both the structural level and the cellular level are simulated by the *finite element method* (FEM). Two levels are fully coupled and computed simultaneously, where the unknown constitutive behaviors on the structure level are represented by the effective behaviors of homogenized *representative volume elements* (RVEs), and the strain states of RVEs are given by the associated integration points. Towards a better understanding of the studied architected SMA, unit cells (RVEs) with different void fractions are introduced to study the superelasticity effect of the materials and structures.

2 Cellular Response

The SMA model, proposed by Chemisky et al. [11], is adopted for the thermomechanical behavior modeling of the architected SMA. This model follows the work of Peultier et al. [12], who proposed a macroscopic phenomenological SMA approach based on the Gibbs free energy. This model was implemented on ABAQUS via *user-defined materials* (UMAT) and validated by experiments. It was later improved by Chemisky and Duval; see Chemisky et al. [11]; Duval et al. [13]. The SMA constitutive model used here is able to describe four different strain mechanisms: the elastic strain ε^e, the thermal expansion strain ε^{th}, the martensitic transformation strain ε^{tr} and the twin accommodation strain ε^{tw}. To this end, the total strain is decomposed in the following form:

$$\varepsilon = \varepsilon^e + \varepsilon^{th} + \varepsilon^{tr} + \varepsilon^{tw}, \tag{1}$$

The implementation of this model in a finite element code is realized, see Chemisky et al. [11] and Duval et al. [13] for more details about the implementation process,

Five types of RVEs with different void volume factions ξ are studied, as illustrated in Figure 1. The size of the cube is given by 1 mm $\times$ 1 mm $\times$ 1 mm. It is formed by excavating cylindrical holes through the center of each face of a cube SMA. Following the constitutive model introduced previously, the material parameters of a conventional NiTi alloy are given in Table 1, which are identified with the experimental data of Sittner et al. [14].

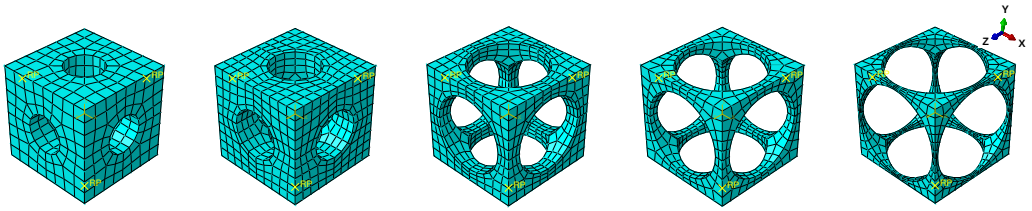

(a) $\xi = 29.1\%$ (b) $\xi = 40.7\%$ (c) $\xi = 72.5\%$ (d) $\xi = 82.2\%$ (e) $\xi = 90.7\%$

Figure 1: Meshes for architected SMA RVEs with different void volume fractions ξ.

Table 1: Material parameters for SMA.

E (MPa)	39,500	B_r (MPa °C^{-1})	7	H_f (MPa)	2
ν	0.3	B_f (MPa °C^{-1})	7	H_{tr} (MPa)	1635
ε^T_{trac}	0.056	M_s (°C)	-80	H_{tw} (MPa)	25,000
ε^{TFA}_{trac}	0.053	A_f (°C)	-2	H_s (MPa)	68.5
ε^T_{comp}	0.044	F_ε (MPa)	220		

According to computational homogenization theory, periodic boundary conditions are introduced into RVE by the *multi-point constraints* (MPCs) on ABAQUS:

$$\Delta\mathbf{u}^+ - \Delta\mathbf{u}^- = \Delta\bar{\varepsilon}\cdot(\mathbf{x}^+ - \mathbf{x}^-) \;\; on \;\; \partial\omega, \tag{2}$$

where $\mathbf{u}$ is the displacement vector, $\mathbf{x}$ is the coordinates of nodes and $\bar{\varepsilon}$ is the strain load applied on RVE. The notations $+$ and $-$ denote the nodes on opposite boundaries; the notation Δ represents the incremental case. A tensile strain up to 10% in the Y direction is applied on RVE at a constant temperature of 30 °C. Figure 2a gives the curves of averaged stress versus the averaged stain along the loading direction, simulated by the above RVEs respectively. The absolute value of stress in different RVEs at a certain strain level increases along with the decreasing of the void volume fraction, as depicted in Figure 2a. Figure 2b gives the martensitic volume fraction averaged over SMA versus the strain averaged over the cube. The martensitic volume fraction $\bar{f}_t$ increases along with the increasing of the strain level, but stops before it reaches one. Namely, each RVE has a certain maximum $\bar{f}_t$ value in this loading case.

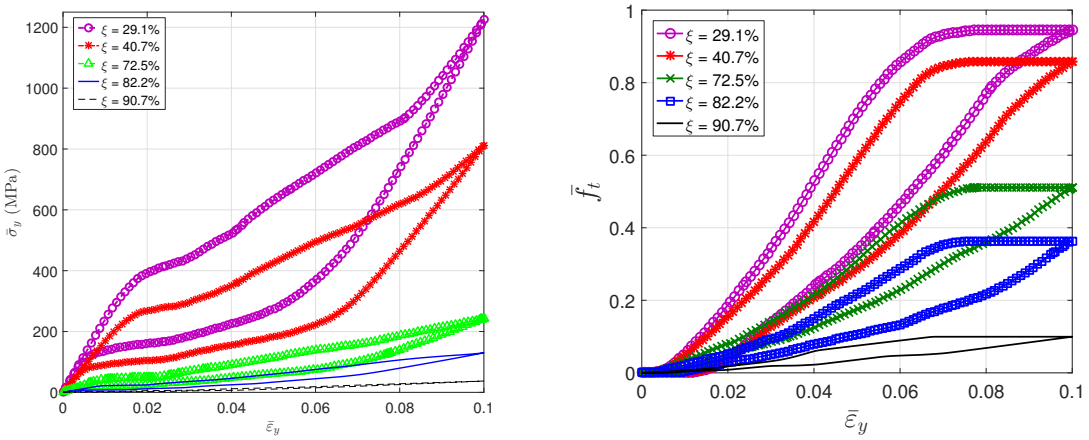

(a) (b)

Figure 2: (a) the evolution of the averaged stress-strain curves simulated by RVEs with different void fractions; (b) the evolution of the martensitic volume fraction versus the averaged strain curves simulated by RVEs with different void fractions.

3 Structural Response

In this section, the structural responses of the architected SMAs are studied by FE^2 which shows good ability in modeling the superelasticity and the shape memory effect of the SMA composites [9, 10]. The constitutive behavior of the macroscopic structure is represented by the computational homogenized RVEs in the last subsection. A 3D beam subjected to three-point bending load is shown in Figure 3.

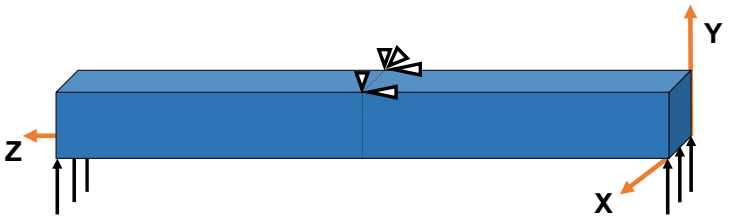

Figure 3: Geometry and boundary conditions for the three-point bending beam.

This beam is composed of architected SMA. The width, length and height of the beam are 5 mm, 20 mm and 5 mm, respectively. Edge Y = 5 mm, Z = 10 mm is fixed in the Y and Z directions. A displacement load up to 0.5 mm in the Y direction is applied on the edges Y = Z = 0 mm and Z = 20 mm, Y = 0 mm. Node X = 0 mm, Y = 5 mm, Z = 10 mm is fixed in the X direction in order to eliminate the rigid body displacement in the X direction. Considering the symmetry of the structure and the boundaries, only the left half of the structure is simulated in order to reduce the computation cost. To do this, an additional displacement constraint in the Z direction is given on face Z = 10 mm. Since the deformation in the X direction is not obvious in the three-point bending test, one element is used in this direction. Each edge in the Y direction is meshed by two elements and in the Z direction by four elements. The continuum 3D solid element with incompatible modes (labeled C3D8I in ABAQUS) is adopted for the modeling of the macroscopic beam since it is enhanced by incompatible modes to improve its bending behavior. The RVEs studied in the last section are used herein with void volume fractions ξ of 40.7%, 72.5% and 82.2%, respectively.

The macroscopic constitutive behavior on each integration point is to be represented by the effective behavior of the associated RVE at each macroscopic increment. A brief flow diagram, showing how this multiscale problem is solved, is illustrated in Figure 4. Specifically, the effective behavior of RVE is computed by seeking the relations between the averaged stresses and averaged strains over the RVE via a series of loading tests. Once the effective behavior is obtained, the macroscopic problem is to be solved. Considering the nonlinear response of the RVE during loading, the macroscopic convergence has to be checked in each macroscopic iteration of the Newton–Raphson framework. In an iteration, the

strain states of RVEs are updated with the macroscopic strains, and in return, the macroscopic stresses are renewed by updating the averaged stress of the RVE at the new strain states.

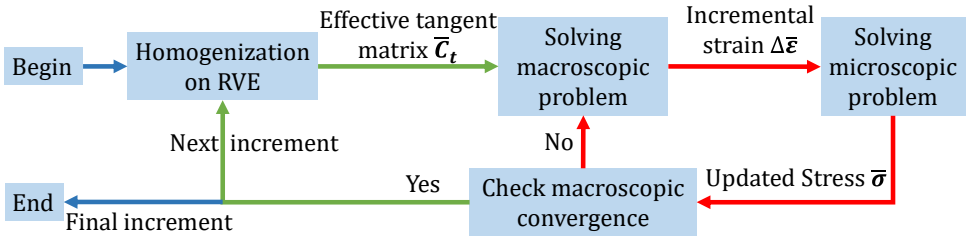

Figure 4: The nonlinear interaction between two scales in the Newton–Raphson framework.

Figure 5 shows the nonlinear response of the macroscopic beam structure with three different void fractions. The linear response is observed at the very beginning, and the microscopic structures deform without any phase transformation. As the loading increases, the forward phase transformation begins over the high stress area of the beam. The structure inherits both the hysteresis effect and the superelasticity from the architected SMA cells.

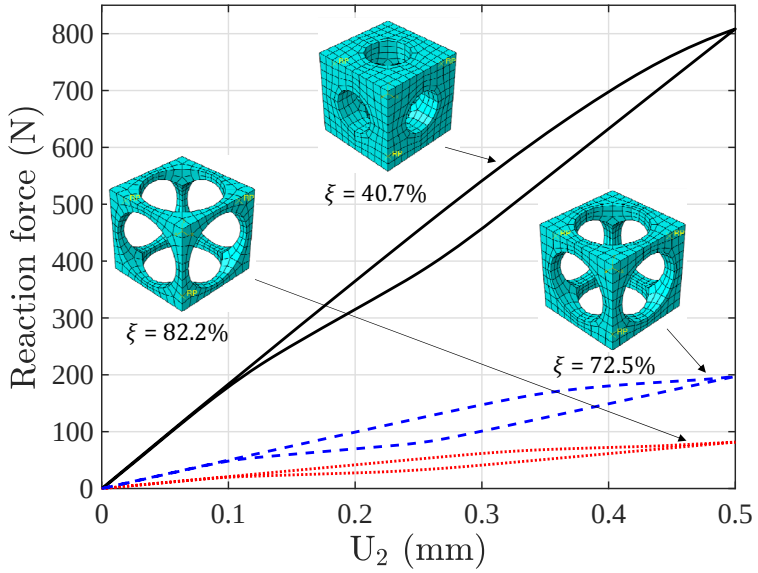

Figure 5: Force-displacement curve of the boundary Z = 20 mm, Y = 0 mm on the bending beam.

4 Conclusion

In this paper, the superelasticity behavior of the architected SMA structure is studied with a 3D multiscale finite element model. The superelasticity responses and the hysteresis effects are observed in RVEs. The effect of changing the void fraction on the stiffness, the maximum martensitic volume fraction and hysteresis effect are discussed in detail. Moreover, a multiscale analysis is carried out to model the structural response, as well as the cellular response. Structural responses with different void fractions are studied, which gives a good reference of the void fractions' influences on structural stiffness and hysteresis.

Acknowledgments

This work has been supported by the French National Research Agency ANR (LabEx DAMAS, Grant No. ANR-11-LABX-0008-01) and the National Natural Science Foundation of China (Grant No. 11772238).

References

[1] T.D. Ngo, A. Kashani, G. Imbalzano, K.T.Q. Nguyen, D. Hui. *Additive manufacturing (3D printing): A review of materials, methods, applications and challenges*, Composite Part B: Structural Engineering, Elsevier, 172–196, 2018.

[2] A. Mostafaei, P.R.D. Vecchis, E.L. Stevens, M. Chmielus. *Sintering regimes and resulting microstructure and properties of binder jet 3D printed Ni-Mn-Ga magnetic shape memory alloys*, Acta Materialia, Elsevier, 355–364, 2018.

[3] E. Patoor, D.C. Lagoudas, P.B. Entchev, L. Catherine Brinson, X. Gao. *Shape memory alloys, Part I: General properties and modeling of single crystals*, Mechanics of Materials, Elsevier, 391–429, 2006.

[4] D.C. Lagoudas, P.B. Entchev, P. Popov, E. Patoor, L. Catherine Brinson, X. Gao. *Shape memory alloys, Part II: Modeling of polycrystals*, Mechanics of Materials, Elsevier, 430–462, 2006.

[5] C. Cisse, W. Zaki, T. Ben Zineb. *A review of constitutive models and modeling techniques for shape memory alloys*, International Journal of Plasticity, Elsevier, 244–284, 2016.

[6] T.A. Schaedler, C.J. Ro, A.E. Sorensen, Z. Eckel, S.S. Yang, W.B. Carter, A.J. Jacobsen. *Designing metallic microlattices for energy absorber applications*, Advanced Engineering Materials, Wiley, 3, 2014.

[7] F. Feyel. *A multilevel finite element method (FE^2) to describe the response of highly non-linear structures using generalized continua*, Computer Methods in Applied Mechanics and Engineering, Elsevier, 3233–3244, 2003.

[8] V.G. Kousnetzova, M.G.D. Geers, W.A.M. Brekelmans. *Multi-scale second-order computational homogenization of multi-phase materials: a nested finite element solution strategy*, Computer Methods in Applied Mechanics and Engineering, Elsevier, 5525–5550, 2004.

[9] R. Xu, C. Bouby, H. Zahrouni, T. Ben Zineb, H. Hu, M. Potier-Ferry. *3D modeling of shape memory alloy fiber reinforced composites by multiscale finite element method*, Composite Structures, Elsevier, 408–419, 2018.

[10] R. Xu, C. Bouby, H. Zahrouni, T. Ben Zineb, H. Hu, M. Potier-Ferry. *A multiscale analysis on the superelasticity behavior of architected shape memory alloy materials*, Materials, MDPI, 1746, 2018.

[11] Y. Chemisky, A. Duval, E. Patoor, T. Ben Zineb. *Constitutive model for shape memory alloys including phase transformation, martensitic reorientation and twins accommodation*, Mechanics of Materials, Elsevier, 361–376, 2011.

[12] B. Peultier, T. Ben Zineb, E. Patoor. *Macroscopic constitutive law of shape memory alloy thermomechanical behaviour. Application to structure computation by FEM*, Mechanics of Materials, Elsevier, 510–524, 2006.

[13] A. Duval, M. Haboussi, T. Ben Zineb. *Modelling of localization and propagation of phase transformation in superelastic SMA by a gradient nonlocal approach*, International Journal of Solids and Structures, Elsevier, 1879–1893, 2011.

[14] P. Sittner, L. Heller, J. Pilch, P. Sedlak, M. Frost, Y. Chemisky, A. Duval, B. Piotrowski, T. Ben Zineb, E. Patoor, et al. *Roundrobin SMA modeling*, In Proceedings of the ESOMAT 2009, Prague, Czech Republic, 2009.